Measuring the absolute Raman cross section of nanographites as a function of laser energy and crystallite size

L. G. Cançado,* A. Jorio, and M. A Pimenta
Departamento de Física, Universidade Federal de Minas Gerais, 30123-970 Belo Horizonte, Brazil
(Received 2 April 2007; revised manuscript received 25 June 2007; published 10 August 2007)

In this paper, the dependence of the differential Raman cross section β of the D, G, D', and G' bands of nanographites on the excitation laser energy and also on the crystallite size is reported. We show that β_G is proportional to the fourth power of the excitation laser energy (E_l), as predicted by the Raman scattering theory. For the bands which arise from the double-resonance mechanism (D, D', and G'), the differential cross section does not depend on E_l, explaining the strong dependence of the ratio I_D/I_G on the excitation laser energy E_l used in the Raman experiment. The L_a dependence of D and D' band differential cross sections is measured, confirming that the proportionality $I_D/I_G \propto L_a^{-1}$ originates from the strong dependence of β_D on the inverse of the crystallite size. In the G' band case, the data show that its differential cross section increases with the increasing crystallite size L_a, following an opposite behavior when compared with the disorder induced D and D' bands. An analysis on the dependence of the full width at half maximum (Γ) of the D, G, D', and G' bands on the crystallite size L_a of nanographites is performed, showing that the phonon lifetime is proportional to the crystallite size.

DOI: 10.1103/PhysRevB.76.064304 PACS number(s): 78.30.−j, 63.22.+m

I. INTRODUCTION

The interest in the Raman spectrum of nanographite structures increased recently with the report on the massless and relativistic properties of the conduction electrons in a single graphene layer responsible for the unusual properties of the quantum Hall effect in this system,[1–3] and the focus is justified by the richness of Raman spectroscopy of graphitic systems. The Raman spectrum of nanographites can be used to determine the in-plane size (L_a) of the crystallites,[4–11] and the disorder-induced bands in the Raman spectrum of a graphite edge can be analyzed in order to identify the local atomic arrangement, defining if the edge has an armchair or zigzag shape.[12] Raman scattering can be used in order to determine if a nanographite sample presents stacking order or turbostratic structure.[13–16] In the case of graphene samples with a few layers, Raman spectroscopy gives a fingerprint for the determination of the number of stacked planes which compose the graphene piece.[17–19]

Besides its many practical applications, Raman scattering in nanographitic systems is also a rich scientific subject, involving resonance conditions and defect-induced processes.[20–24] The intensities of the features present in the Raman spectrum of nanographites are known to be strongly dependent on their structural (defect-related) properties. The ratio between the intensities (integrated areas) of the disorder-induced D band ($\sim$1350 cm^{-1}) and the first-order allowed G band ($\sim$1580 cm^{-1}) is inversely proportional to the crystallite size L_a of nanographites, that is, $I_D/I_G \propto 1/L_a$.[4–8] Another remarkable characteristic in the Raman spectrum of nanographites is the strong dependence of the ratio I_D/I_G on the excitation laser energy E_l used in the Raman experiment, i.e., $I_D/I_G \propto E_l^{-4}$.[7,8] These properties have attracted the attention of many theoretical and experimental groups to the theme.[9,10,20–28]

Despite the large amount of experimental data available in the literature concerning the values of the ratio I_D/I_G,[6–11] the experimental study of the absolute intensities of the D and G Raman bands of nanographite systems is still missing. In this case, the origin of the dependence of the ratio I_D/I_G on the excitation laser energy could not be surely explained until now, since the dependence of the G and D band absolute intensities on E_l are both unknown. In this paper, an experimental study of the absolute Raman cross section of the main features in the Raman spectrum of nanographite samples with different crystallite sizes L_a and using different values of excitation laser energies (in the visible range) is presented. The analysis includes the disorder-induced D' band[29] ($\sim$1620 cm^{-1}) and the two-phonon band associated with the D band, the so-called G' band, occurring at $\sim$2700 cm^{-1}.[30,31] The samples have no stacking order and present well defined crystallite borders, being considered as prototypes of two-dimensional nanographite systems.[7,16] The Raman data obtained reveal the dependence of the absolute intensities β_D and β_G on the crystallite size and excitation laser energy E_l for nanographites, showing that the dependence of the ratio I_D/I_G on E_l is caused by a deviation of the D band intensity from the ω^4 dependence predicted by the Raman scattering theory.[32–40] The absolute differential cross section for the G' band is also obtained, giving support to the analysis of the D band intensity dependence on the excitation laser energy and indicating that such a deviation from the ω^4 dependence occurs for those bands which originate from the double-resonance process. Moreover, this result indicates that the deviation of the D and D' intensities from the ω^4 dependence cannot be associated with the electron-defect interaction matrix elements. The L_a dependence of D and D' band differential cross sections is measured, confirming that the proportionality $I_D/I_G \propto L_a^{-1}$ originated from the strong dependence of β_D on the inverse of the crystallite size. The data allow us to establish a general equation giving the dependence of the ratio $I_{D'}/I_G$ on the excitation laser energy and crystallite size L_a. In contrast with the disorder-induced D and D' bands, the results show that the differential cross

section of the G' band increases with increasing crystallite size L_a. An analysis of the dependence on the full width at half maximum (Γ) of the D, G, D', and G' bands on the crystallite size L_a of nanographites is performed, showing that the phonon lifetime is proportional to the crystallite size.

II. EXPERIMENTAL DETAILS

The Raman spectra of nanographites were measured in a Dilor XY spectrometer setup, using five excitation laser energies, E_l=1.92, 2.18, 2.41, 2.54, and 2.71 eV. The samples were nanographite films with average in-plane crystallite sizes L_a=20, 35, and 65 nm (for details about the synthesis of the samples and measurement of the crystallite sizes, see Ref. 7). The small linewidths Γ observed for the disorder-induced D and D' bands (shown in Sec. VII) indicate that the samples have a narrow crystallite size distribution (see linewidths for spectra at Refs. 4 and 5 for comparison). This fact is also supported by the scanning tunneling microscopy (STM) study of the samples reported in Ref. 7. Previous x-ray diffraction and Raman spectroscopy analyses have shown that these samples do not present stacking order but, instead, have a turbostratic structure.[16] The spectrometer intensity calibration was performed using a standard LS-1-CAL-INT tungsten halogen calibrated light source provided by NIST. The absolute values of the differential Raman cross section were obtained by comparison with those obtained from the Raman bands of the cyclohexane liquid (C_6H_{12}), for which the dependence of the absolute Raman cross sections is known from the literature.[41] The Raman spectra of the nanographite samples were obtained under the same conditions, with a fixed incident laser intensity I_0=6.25 $\times 10^8$ mW/cm^2 and accumulation time t=60 s.

III. EXCITATION LASER ENERGY DEPENDENCE FOR THE ABSOLUTE RAMAN CROSS SECTION OF NANOGRAPHITES

Figure 1 shows the calibrated Raman spectra (spectral differential cross section β') of the nanographite sample with L_a=35 nm, obtained using the five distinct values of E_l after applying the procedure necessary for the intensity calibration process. The graphic shows an increase on the G band intensity with the excitation laser energy. For the D, D', and G' bands, the spectral differential cross section is roughly constant.

Figures 2(a)–2(c) show the differential cross section β (integrated area) for D, G, and D' bands vs the excitation laser energy E_l, obtained from the samples with L_a=20 nm [Fig. 2(a)], L_a=35 nm [Fig. 2(b)], and L_a=65 nm [Fig. 2(c)]. It is clear in Fig. 2 that the differential cross sections of the disorder-induced D and D' bands do not depend considerably on the excitation laser energy. On the other hand, the differential cross section of the G band increases with increasing excitation laser energy. Considering that the differential Raman cross section is predicted to follow the proportionality $\beta \propto E_l^4 |W|^2$ in the so-called ω^4 dependence,[44] where W is the microscopic amplitude probability obtained from the time dependent perturbation theory,[32–40] the solid curves

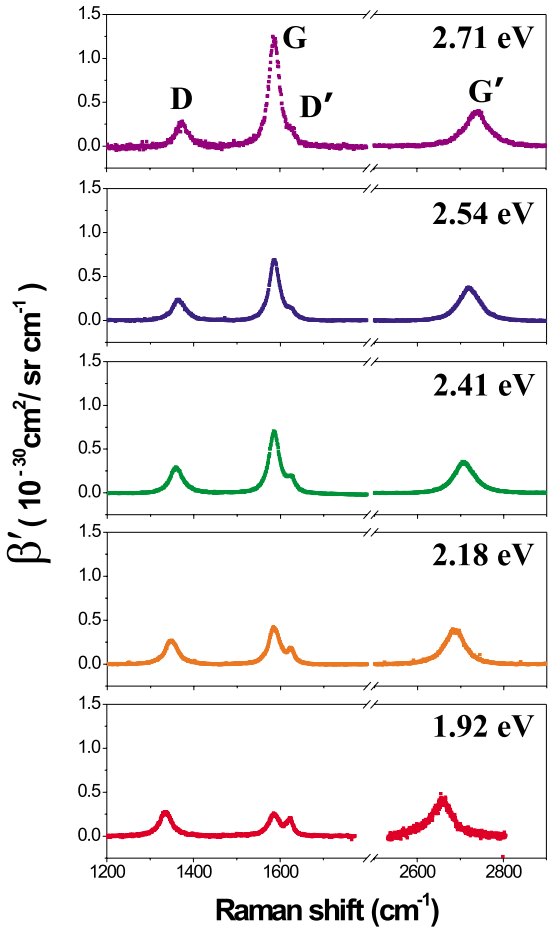

FIG. 1. (Color online) The spectral differential cross section of the D, G, D', and G' bands for the nanographite sample with L_a=35 nm, using five different values of E_l (indicated at the top of each spectrum). The same vertical scale was used for the five spectra for comparison.

in Figs. 2(a)–2(c) are the fits for the G band (β_G) data, $\beta_G \propto E_l^4$, in agreement with the theory of Raman scattering.

In contrast to the G band data, the experimental data for the D and D' bands in Figs. 2(a)–2(c) indicate that β_D and $\beta_{D'}$ do not follow the ω^4 dependence. In fact, deviation from the ω^4 dependence occurs for bands originated from resonance processes in which the matrix elements composing the amplitude probability W carry some dependence on E_l.[42] These results show that the dependence of the ratio I_D/I_G on the excitation laser energy observed by many authors[7,8,11] comes from the fact that the G band differential cross section is proportional to E_l^4 and that the D band differential cross section does not change with the excitation laser energy.

The mechanism giving rise to the G band is quite different from that giving rise to the D and D' bands. The G band is a first-order allowed band originated from the doubly degenerated vibrational mode Γ_6^+ (E_{2g}) that occurs at the crossing of the iLO and iTO phonon branches at the Γ point in the first Brillouin zone of graphite.[4,5] The D and D' scatterings are defect-induced double-resonance processes which become Raman active at the borders of the graphite crystallites due to loss of translational symmetry.[4,5,23,24] Therefore, the differen-

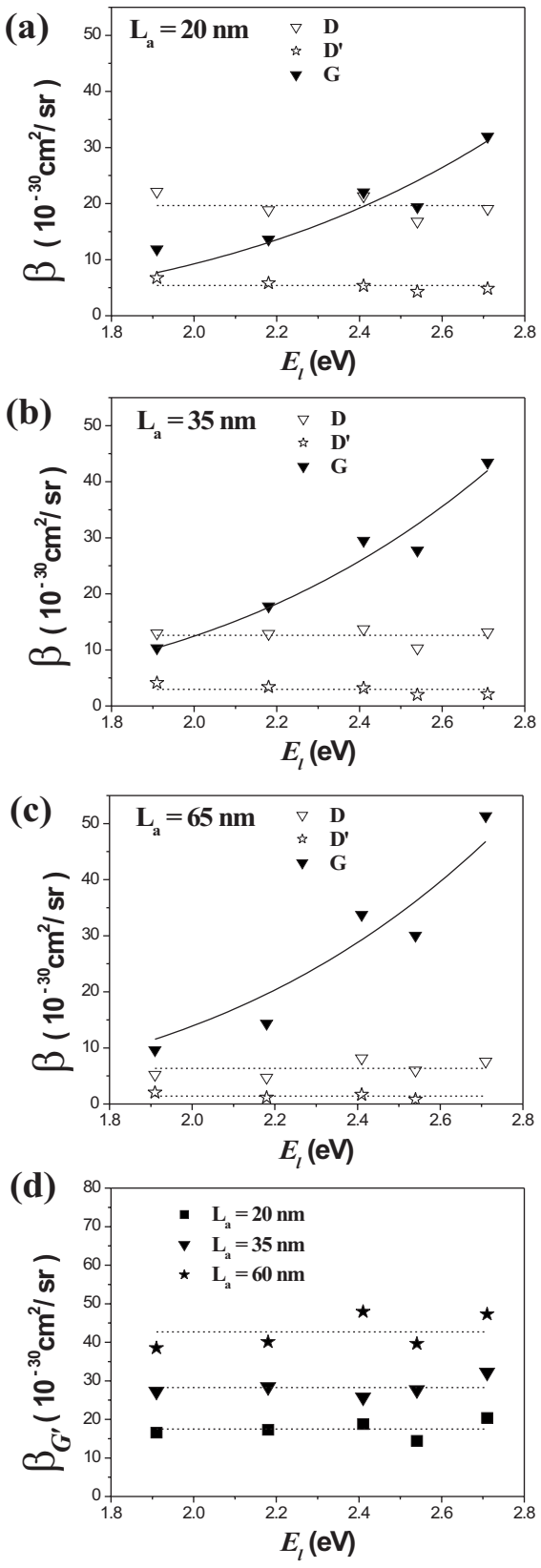

FIG. 2. The differential cross section of the D, G, and D' bands vs the excitation laser energy E_l, obtained from the samples with (a) L_a=20 nm, (b) L_a=35 nm, and (c) L_a=65 nm. (d) The differential cross section of the G' band vs the excitation laser energy, for the samples with crystallite sizes L_a=20, 35, and 65 nm.

tial Raman cross section for the D and D' bands includes an additional matrix element term associated with the electron-defect interaction Hamiltonian, which is absent in the G band differential cross section.[23,24] In order to check if the deviation from the ω^4 dependence observed for the D and D' band absolute intensities is associated with the electron-defect interaction matrix element, we have also measured the G' band absolute intensity. The G' band is the overtone of the D band, and it does not require a disorder-induced process to become active, since momentum conservation is guaranteed in two-phonon Raman processes. Figure 2(d) shows the measured values of $\beta_{G'}$ vs the excitation laser energy for the samples with crystallite sizes L_a=20, 35, and 65 nm. As depicted in Fig. 2(d), $\beta_{G'}$ is affected by the crystallite size L_a, but it does not depend on the excitation laser energy, similar to the case of the D and D' bands. This result indicates that the deviation of the D and D' intensities from the ω^4 dependence is not associated with the electron-defect interaction matrix elements.

These results are in agreement with the recent work where the square modulus of the transition probability $|W|^2$ is predicted to be proportional to ω_l^{-4} for the D band scattering.[28] Therefore, the square modulus of the transition probability cancels the ω^4 dependence for the D band cross section. It is also shown in this work that the dependence on ω_l^{-4} of the square modulus of the transition rate for the D band scattering comes from the electron-radiation coupling matrix element in the double-resonance process of spatially confined nanographites. Since the D' and G' bands are also generated by a double-resonance mechanism, this result should also apply, in agreement with the observations reported in this section.

IV. CRYSTALLITE SIZE L_a DEPENDENCE FOR THE DIFFERENTIAL CROSS SECTIONS OF THE DISORDER-INDUCED D AND D' BANDS

The borders of the crystallites work as defects involved in the double-resonance process, giving rise to the D and D' bands in the Raman spectra of nanographites.[12] Therefore, the D and D' band differential cross sections are expected to be proportional to the amount of crystallite boundary in the nanographite sample, which means that they should be inversely proportional to the crystallite size L_a. Figure 3 shows the plot of the D (filled symbols) and D' (open symbols) band differential cross sections vs the inverse of the crystallite size L_a, using the five values of E_l. The plot shows that both β_D and $\beta_{D'}$ are linearly proportional to $1/L_a$, as predicted by Tuinstra and Koenig for the D band scattering.[4,5] The dependencies of β_D and $\beta_{D'}$ on $1/L_a$ were quantified from the linear fits depicted in Fig. 3 (solid line for the D band data, and dashed line for the D' data), giving $\beta_D = 405/L_a$ and $\beta_{D'} = 115/L_a$, respectively, where β_D and $\beta_{D'}$ are given in 10^{-30} cm^2/sr and L_a is given in nanometers.

Although the ratio I_D/I_G in nanographitic systems has been measured previously by many groups,[6–11] our measurement of the D band differential cross section shows that the proportionality $I_D/I_G \propto L_a^{-1}$ originated from the strong dependence of β_D on the inverse of the crystallite size.

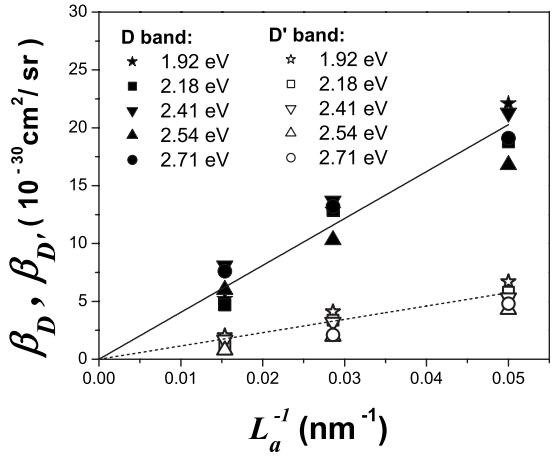

FIG. 3. Plot of the D (filled symbols) and D' (open symbols) band differential cross sections vs the inverse of the crystallite size L_a, obtained using the five values of E_l.

V. L_a AND E_l DEPENDENCIES OF THE RATIOS β_D/β_G AND $\beta_{D'}/\beta_G$

Figure 4 shows the plot of the ratios β_D/β_G (solid squares) and $\beta_{D'}/\beta_G$ (empty squares) vs the inverse of the product $E_l^4 L_a$ for the data depicted in Figs. 2(a)–2(c). The lines (solid and dashed lines for the D and D' band data, respectively) are linear plots giving the following relations:

$$\frac{\beta_D}{\beta_G} = \frac{560}{L_a E_l^4} \tag{1}$$

and

$$\frac{\beta_{D'}}{\beta_G} = \frac{160}{L_a E_l^4}, \tag{2}$$

where L_a and E_l are in nanometers and eV, respectively. While Eq. (1) confirms our result previously reported in Ref. 7, Eq. (2) gives an expression associating the crystallite size L_a with the ratio $\beta_{D'}/\beta_G$, for experiments using any excitation laser energy in the visible range.

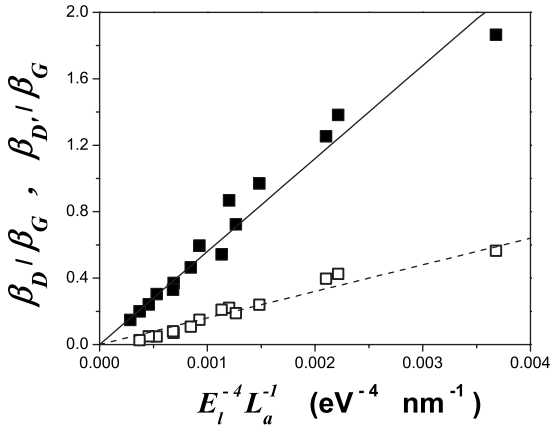

FIG. 4. Plot of the ratios β_D/β_G (solid squares) and $\beta_{D'}/\beta_G$ (empty squares) vs the inverse of the product $E_l^4 L_a$, for the whole data obtained in the experiment. The lines (solid and dashed lines for the D and D' band data, respectively) are the linear fit originating Eqs. (1) and (2).

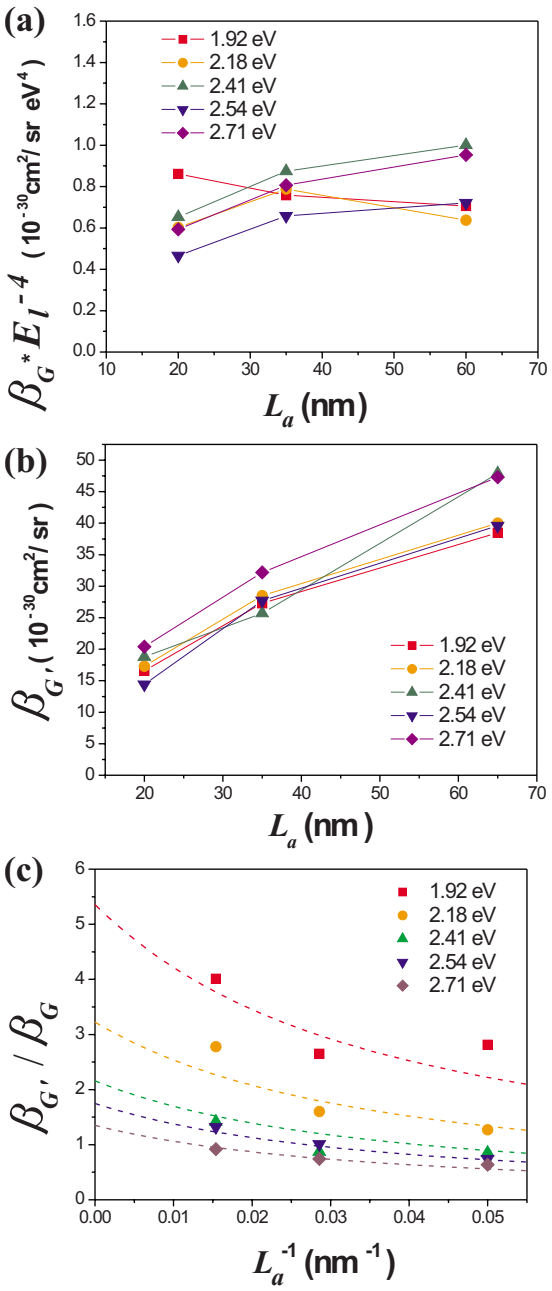

FIG. 5. (Color online) (a) Plot of the product $\beta_G E_l^{-4}$ vs the crystallite size L_a. (b) The differential cross section of the G' band vs the crystallite size L_a. (c) The ratio $\beta_{G'}/\beta_G$ vs the inverse of the crystallite size L_a, for the data obtained using five different values of E_l.

VI. CRYSTALLITE SIZE L_a DEPENDENCE OF THE G AND G' BAND DIFFERENTIAL CROSS SECTIONS

Figure 5(a) shows the plot of the product $\beta_G E_l^{-4}$ vs the crystallite size L_a. It is clear in Fig. 5(a) that, by excluding the dependence of the absolute cross section of the G band on the excitation laser energy, the G band absolute intensity

does not depend considerably on the crystallite size L_a.

Figure 5(b) shows the plot of the differential cross section of the G' band vs the crystallite size L_a. As shown in Fig. 5(b), the absolute intensity of the G' band has a direction opposite to that followed by the D and D' bands, since $\beta_{G'}$ becomes stronger with increasing L_a. These results should not be associated with the amount of carbon material under illumination, since the sample completely fills the laser focus in all cases.

Figure 5(c) shows the plot of the ratio $\beta_{G'}/\beta_G$ with the inverse of the crystallite size L_a, for the data obtained using five different values of E_l. The extrapolation of the experimental data for an infinite graphene crystal [dashed lines in Fig. 5(c)] shows that the absolute intensity of the G' band is larger than the absolute intensity of the G band, the value of the ratio $\beta_{G'}/\beta_G$ estimated to be about 2.5 and 5 for experiments using the 2.41 and 1.92 eV excitation laser lines, respectively. These values are in good agreement with the results obtained from Refs. 17–19 for micron-sized graphene samples, showing that the strong dependence of the G' band on the crystallite size L_a gives rise to the relatively high values of the ratio $\beta_{G'}/\beta_G$ observed in these systems.

VII. CRYSTALLITE SIZE L_a DEPENDENCE OF THE FULL WIDTH AT HALF MAXIMUM

Figure 6 shows the plot of the full width at half maximum (FWHM) Γ for the D, D', G, and G' bands [Figs. 6(a), 6(b), 6(c), and 6(d), respectively] vs the crystallite size observed in the Raman spectra taken from the samples with L_a=20, 35, and 65 nm, using five different values for the excitation laser energy E_l. The linear fits [dashed lines in Figs. 6(a)–6(d)] show that Γ is proportional to $1/L_a$ for the D, D', G, and G' bands and does not depend significantly on E_l. The linear fit parameters A and B are given in Table I, where the notation $\Gamma = A + BL_a^{-1}$ has been used. It is interesting to note that the slope parameter B is similar for the one-phonon process bands ($\sim$550 cm^{-1} nm) and approximately twice for the two-phonon G' band process (1000 cm^{-1} nm).

The proportionality between Γ and $1/L_a$ observed in Fig. 6 can be discussed in the following terms: If the crystallite size is smaller than the phonon mean free path, the phonon lifetime τ will be proportional to the crystallite size L_a. Since the FWHM is determined by lifetime effects in Raman bands involving resonance conditions,[43] we have $\Gamma \propto 1/\tau$ and, consequently, $\Gamma \propto 1/L_a$.

We must consider that the phonon lifetime can be shorter for samples with small L_a due to the presence of defects in the crystallites, increasing the probability for the phonon-defect scattering. However, it does not seem to occur in the present case. First, the relatively small linewidth of the Raman bands obtained from the samples used in this experiment, when compared with those obtained from samples with similar values of the ratio I_D/I_G reported in other works (see linewidths for spectra at Refs. 4 and 5 for comparison), gives evidence that the samples used here exhibit a low density of defects inside the crystallites. Moreover, Fig. 7 shows two STM images, with atomic resolution, obtained from the surface of a crystallite at the sample with L_a=65 nm. The

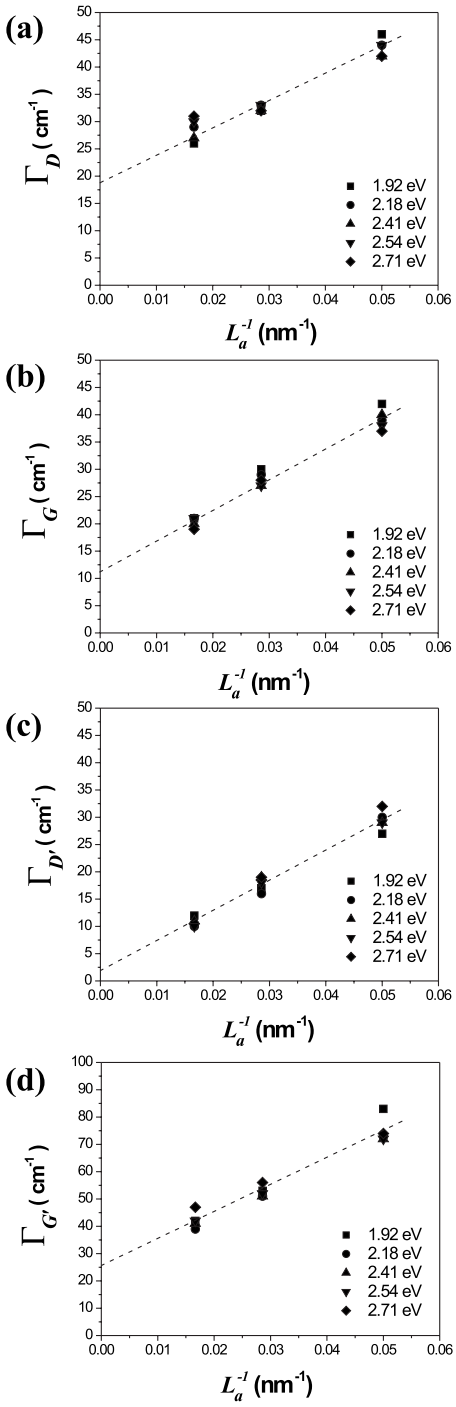

FIG. 6. The full width at half maximum Γ for the D, D', G, and G' bands [(a), (b), (c), and (d), respectively] vs the crystallite size observed in the Raman spectra taken from the samples with L_a =20, 35, and 65 nm, using five different values for the excitation laser energy E_l.

atomic arrangement of the carbon atoms observed in these pictures indicates that the samples are actually formed by nanographitic crystallites instead of disordered carbon. Finally, another strong evidence that the size of the crystallites actually defines the phonon lifetime is the value of parameter A in Table I. Considering that the FWHM obtained here is due to the finite size of the crystallites, parameter A corre-

TABLE I. The linear fit parameters A and B, where the notation $\Gamma = A + BL_a^{-1}$ was used, obtained from the plot of the full width at half maximum Γ for the D, D', G, and G' bands depicted in Figs. 6(a)–6(d), respectively.

	A (cm^{-1})	B (cm^{-1} nm)
Γ_D	19	500
Γ_G	11	560
$\Gamma_{D'}$	2	550
$\Gamma_{G'}$	26	1000

sponds to the extrapolation for the value of the FWHM of the respective band obtained from the Raman spectrum of a sample with an infinite L_a. In fact, the values of A obtained here are very close to the FWHM values recently reported in Refs. 17–19 for the Raman bands obtained from micron-sized graphene samples.

VIII. FINAL REMARKS

In summary, we have reported in this paper the dependence of the absolute differential cross section β of the D, G, D', and G' bands on the excitation laser energy (in the visible range) and also on the crystallite size. We show that β_G is proportional to the fourth power of the excitation laser energy, as predicted by the Raman scattering theory. For the bands arising from the double-resonance mechanism (D, D', and G'), the absolute differential cross section does not depend on E_l. The results show that the dependence of the ratio I_D/I_G on E_l is caused by a deviation of the D band intensity from the ω^4 dependence predicted by the Raman scattering theory. The L_a dependence of D and D' band absolute differential cross sections is measured, confirming that the proportionality $I_D/I_G \propto L_a^{-1}$ originates from the strong dependence of β_D on the inverse of the crystallite size. The same treatment shows a strong enhancement of the absolute differential cross section of the G' band with increasing crystallite size L_a. An analysis on the dependence of the full width at half maximum (Γ) of the D, G, D', and G' bands on L_a of nanographites is performed, showing that the phonon lifetime is proportional to the crystallite size.

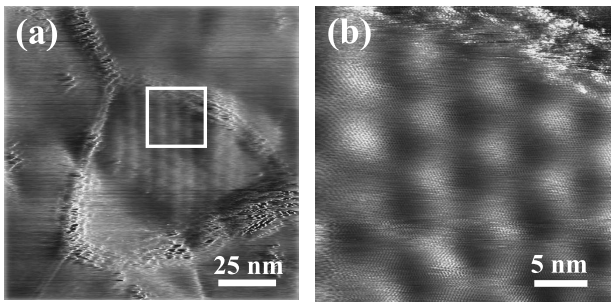

FIG. 7. Scanning tunneling microscopy (STM) images, with atomic resolution, obtained from the surface of a crystallite of the sample with L_a=65 nm. (a) A Moire pattern at the crystallite surface is observed. (b) Magnification of the region delimited by the white square in (a), where the carbon atom positions in the graphite lattice can be observed. The STM measurements were performed using a Nanoscope II MultiMode microscope from Digital Instruments. For more details, see Ref. 7.

ACKNOWLEDGMENTS

This work was supported by the Brazilian Network on Carbon Nanotube Research-MCT and FAPEMIG. L.G.C. acknowledges the support from the Brazilian Agency CNPq.

*cancado@optics.rochester.edu

[1] Y. Zhang, Y. W. Tan, H. L. Stormer, and P. Kim, Nature (London) **438**, 201 (2005).
[2] K. S. Novoselov, A. K. Geim, S. V. Morozov, D. Jiang, Y. Zhang, S. V. Dubonos, I. V. Grigorieva, and A. A. Firsov, Science **306**, 5296 (2004).
[3] K. S. Novoselov, A. K. Geim, S. M. Morozov, D. Jiang, M. I. Katsnelson, I. V. Grigorieva, S. V. Dubonos, and A. A. Firsov, Nature (London) **438**, 197 (2005).
[4] F. Tuinstra and J. L. Koenig, J. Chem. Phys. **53**, 1126 (1970).
[5] F. Tuinstra and J. L. Koenig, J. Compos. Mater. **4**, 492 (1970).
[6] D. S. Knight and W. White, J. Mater. Res. **4**, 385 (1989).
[7] L. G. Cançado, K. Takai, T. Enoki, M. Endo, Y. A. Kim, H. Mizusaki, A. Jorio, L. N. Coelho, R. Magalhães-Paniago, and M. A. Pimenta, Appl. Phys. Lett. **88**, 163106 (2006).
[8] T. P. Mernagh, R. P. Cooney, and R. A. Johnson, Carbon **22**, 39 (1984).
[9] A. C. Ferrari and J. Robertson, Phys. Rev. B **61**, 14095 (2000).
[10] A. C. Ferrari and J. Robertson, Phys. Rev. B **64**, 075414 (2001).
[11] Y. Wang, D. C. Alsmeyer, and R. L. McCreery, Chem. Mater. **2**, 557 (1990).
[12] L. G. Cançado, M. A. Pimenta, B. R. A. Neves, M. S. S. Dantas, and A. Jorio, Phys. Rev. Lett. **93**, 247401 (2004).
[13] P. Lespade, A. Marchand, M. Couzi, and F. Cruege, Carbon **22**, 375 (1984).
[14] H. Wilhelm, M. Lelaurain, E. McRae, and B. Humbert, J. Appl. Phys. **84**, 6552 (1998).
[15] E. B. Barros, N. S. Demir, A. G. Souza Filho, J. Mendes Filho, A. Jorio, G. Dresselhaus, and M. S. Dresselhaus, Phys. Rev. B **71**, 165422 (2005).
[16] L. G. Cançado, K. Takai, T. Enoki, M. Endo, Y. A. Kim, H. Mizusaki, A. Jorio, N. L. Speziali, and M. A. Pimenta (unpublished).
[17] A. C. Ferrari, J. C. Meyer, V. Scardaci, C. Casiraghi, M. Lazzeri, F. Mauri, S. Piscanec, D. Jiang, K. S. Novoselov, S. Roth, and A. K. Geim, Phys. Rev. Lett. **97**, 187401 (2006).
[18] A. Gupta, G. Chen, P. Joshi, S. Tadigadapa, and P. C. Eklund, Nano Lett. **6**, 2667 (2006).
[19] D. Graf, F. Molitor, K. Ensslin, C. Stampfer, A. Jungen, C. Hierold, and L. Wirtz, Nano Lett. **7**, 238 (2007).
[20] A. V. Baranov, A. N. Bekhterev, Y. S. Bobovich, and V. I. Petrov, Opt. Spectrosc. **62**, 612 (1987).

[21] I. Pócsik, M. Hundhausen, M. Koós, and L. Ley, J. Non-Cryst. Solids **230**, 1083 (1998).
[22] M. J. Matthews, M. A. Pimenta, G. Dresselhaus, M. S. Dresselhaus, and M. Endo, Phys. Rev. B **59**, R6585 (1999).
[23] C. Thomsen and S. Reich, Phys. Rev. Lett. **85**, 5214 (2000).
[24] R. Saito, A. Jorio, A. G. Souza Filho, G. Dresselhaus, M. S. Dresselhaus, and M. A. Pimenta, Phys. Rev. Lett. **88**, 027401 (2002).
[25] L. G. Cançado, M. A. Pimenta, R. Saito, A. Jorio, L. O. Ladeira, A. Grueneis, A. G. Souza-Filho, G. Dresselhaus, and M. S. Dresselhaus, Phys. Rev. B **66**, 035415 (2002).
[26] P. H. Tan, Y. M. Deng, and Q. Zhao, Phys. Rev. B **58**, 5435 (1998).
[27] S. Reich and C. Thomsen, in *Raman Spectroscopy of Graphite*, edited by The Royal Society, special issue of Philos. Trans. R. Soc. London, Ser. A **362**, 2271 (2004).
[28] S. Oyama, J. Jiang, L. G. Cançado, M. A. Pimenta, A. Jorio, Ge. G. Samsonidze, G. Dresselhaus, and M. S. Dresselhaus, Chem. Phys. Lett. **427**, 117 (2006).
[29] R. Tsu, J. H. Gonzalez, and I. C. Hernandez, Solid State Commun. **27**, 507 (1978).
[30] R. J. Nemanich and S. A. Solin, Solid State Commun. **23**, 417 (1977).
[31] R. J. Nemanich and S. A. Solin, Phys. Rev. B **20**, 392 (1979).
[32] R. Loudon, Adv. Phys. **50**, 813 (2001).
[33] A. K. Ganguly and J. L. Birman, Phys. Rev. **162**, 806 (1967).
[34] José Menendéz and M. Cardona, Phys. Rev. B **31**, 3696 (1985).
[35] A. Cantarero, C. Trallero-Giner, and M. Cardona, Phys. Rev. B **39**, 8388 (1989).
[36] C. Trallero-Giner, A. Cantarero, and M. Cardona, Phys. Rev. B **40**, 4030 (1989).
[37] A. Cantarero, C. Trallero-Giner, and M. Cardona, Phys. Rev. B **40**, 12290 (1989).
[38] A. Alexandrou, C. Trallero-Giner, A. Cantarero, and M. Cardona, Phys. Rev. B **40**, 1603 (1989).
[39] V. I. Gavrilenko, D. Martínez, A. Cantarero, M. Cardona, and C. Trallero-Giner, Phys. Rev. B **42**, 11718 (1990).
[40] C. Trallero-Giner, A. Cantarero, M. Cardona, and M. Mora, Phys. Rev. B **45**, 6601 (1992).
[41] M. O. Trulson and R. A. Mathies, J. Chem. Phys. **84**, 2068 (1986).
[42] H. A. Szymanski, *Raman Spectroscopy* (Plenum, New York, 1987).
[43] R. M. Martin and L. M. Falicov, in *Light Scattering in Solids I: Introductory Concepts*, edited by M. Cardona, Topics in Applied Physics Vol. 8 (Springer, Berlin, 1983).
[44] In fact, the theory of Raman scattering predicts that the Raman cross section is proportional to the third power of the frequency of the scattered light (ω_s) times the frequency of the excitation laser beam (ω_l), that is, $\beta \propto \omega_s^3 \omega_l$. However, since the frequency of the phonon is about ten times smaller than the frequencies of the excitation laser and scattered light beams, we consider that the absolute Raman intensity is proportional to the fourth power of the excitation laser frequency (energy).